doi:10.1016/j.jmb.2007.06.004 *J. Mol. Biol.* (2007) **371**, 1075–1083

JMB

Available online at www.sciencedirect.com

ScienceDirect

ELSEVIER

The Crystal Structure of MCAT from *Mycobacterium tuberculosis* Reveals Three New Catalytic Models

Zexuan Li[1,2], Yishu Huang[3], Jing Ge[4], Hang Fan[1,2], Xiaohong Zhou[1,2] Shentao Li[6], Mark Bartlam[1,2,5], Honghai Wang[3]* and Zihe Rao[1,2,5]*

[1]*Tsinghua-Nankai-IBP Joint Research Group for Structural Biology, Tsinghua University Beijing 100084, China*

[2]*National Laboratory of Biomacromolecules, Institute of Biophysics, Chinese Academy of Sciences, Beijing 100101 China*

[3]*State Key Laboratory of Genetic Engineering, Institute of Genetics, School of Life Sciences, Fudan University Shanghai 200433, China*

[4]*Department of Microbiology and Microbial Engineering School of Life Sciences Fudan University Shanghai 200433, China*

[5]*College of Life Sciences Nankai University Tianjin 300071, China*

[6]*Capital Medical University Beijing 100069, China*

**Corresponding authors*

The malonyl coenzyme A (CoA)-acyl carrier protein (ACP) transacylase (MCAT) plays a key role in cell wall biosynthesis in *Mycobacterium tuberculosis* and other bacteria. The *M. tuberculosis* MCAT (*Mt*MCAT) is encoded by the FabD gene and catalyzes the transacylation of malonate from malonyl-CoA to holo-ACP. Malonyl-ACP is the substrate in fatty acid biosynthesis and is a by-product of the transacylation reaction. This ability for fatty acid biosynthesis enables *M. tuberculosis* to survive in hostile environments, and thus understanding the mechanism of biosynthesis is important for the design of new anti-tuberculosis drugs. The 2.3 Å crystal structure of *Mt*MCAT reported here shows that its catalytic mechanism differs from those of *Sc*MCAT and *Ec*MCAT, whose structures have previously been determined. In *Mt*MCAT, the C^{β}–O^{γ} bond of Ser91 turns upwards, resulting in a different orientation and thus an overall change of the active pocket compared to other known MCAT enzymes. We identify three new nucleophilic attack chains from the *Mt*MCAT structure: His90-Ser91, Asn155-Wat6-Ser91 and Asn155-His90-Ser91. Enzyme activity assays show that His90A, Asn155A and His90A-Asn155A mutants all have substantially reduced MCAT activity, indicating that *M. tuberculosis* MCAT supports a unique means of proton transfer. Furthermore, His194 cannot form part of a His-Ser catalytic dyad and only stabilizes the substrate. This new discovery should provide a deeper insight into the catalytic mechanisms of MCATs.

Keywords: malonyl-CoA:ACP transacylase; crystal structure; nucleophilic attack; fatty acids biosynthesis; *Mycobacterium tuberculosis*

Introduction

Tuberculosis (TB) is caused by the bacterium *Mycobacterium tuberculosis* and poses a serious threat to public health worldwide. TB is responsible for nearly two million deaths annually, while a third of the global population is currently infected with the TB bacillus and more than eight million new cases are diagnosed each year. The case-fatality rate for TB can reach up to 50%, and the situation has been exacerbated by a significant increase in multiple-drug-resistant TB and synergism between Human Immunodeficiency Virus (HIV) and *M. tuberculosis* infection. Considerable research has been directed towards understanding the pathology, molecular mechanism, and drug resistance of TB in order to discover new pharmacological targets†.

Abbreviations used: CoA, coenzyme A; ACP, acyl carrier protein; MCAT, malonyl CoA ACP transacylase; TB, tuberculosis; *Mt*, *Mycobacterium tuberculosis*; *Ec*, *Escherichia coli*; *Sc*, *Streptomyces coelicolor*.

E-mail addresses of the corresponding authors: raozh@xtal.tsinghua.edu.cn; hhwang@fudan.edu.cn

†http://www.wadsworth.org/databank/mycotubr.htm

The impermeable nature of the *M. tuberculosis* cell wall determines cell survival and replication within the hostile environment of host macrophages, which produce microbicidal molecules that are usually sufficient to kill other bacteria.[1] The mycobacterial mycolic acid in *M. tuberculosis*, which is the largest fatty acid in nature, contributes a greater density to the mycobacterial cell envelope, the lipid bilayer outer membrane and the inner leaflet than in other bacterium.[2] Due to the essential role of mycolic acids in intracellular survival of *M. tuberculosis*, the biosynthesis and assembly of these structures has become a promising target in the discovery of antibacterial agents. Several components of the mycolic acid biosynthetic pathway, such as enoyl-ACP reductase, have already been reported as targets for important anti-tuberculosis drugs.[3–7]

As an essential pathway and the first stage in membrane biogenesis, fatty acid biosynthesis is catalyzed by different enzymes according to different species. These enzymes can be divided into two types. In the type I (FAS I) system found in eukaryotes, the biosynthesis of fatty acids is catalyzed by a single large, multifunctional polypeptide. However, in the type II (FAS II) system found in most bacteria, the reactions are carried out by a series of small, soluble proteins that are each encoded by discrete genes.[8,9] Due to the monofunctional nature of type II enzymes, they are more attractive targets for the discovery of antibacterial agents than type I.

The malonyl-CoA:acyl carrier protein transacylase (MCAT, EC 2.3.1.39) is a key enzyme in the FAS II pathway and is responsible for transferring the malonyl group from malonyl-CoA to the holo-ACP *via* formation of free CoASH and malonyl-ACP, which is the substrate required for the elongation steps in fatty acid biosynthesis. In fact, MCAT induces an upstream reaction and may be the essential building block in the fatty acid biosynthesis cycle. In addition, MCAT can provide acyl-ACP thioesters for the biosynthesis of aromatic polyketides.[10–12] Based on its pivotal role in *M. tuberculosis* and other deadly bacteria, MCAT has become one of the most promising targets to either inhibit or kill *M. tuberculosis*. The first inhibitor of MCAT from *Helicobacter pylori* (*Hp*MCAT) has recently been reported. A natural product called corytuberine was discovered to inhibit *Hp*MCAT with an IC_{50} value of 33.1(±3.29) μM. Further enzymatic assay results indicate that corytuberine inhibits *Hp*MCAT in an non-competitive manner.[13]

In *M. tuberculosis*, the FabD (Rv2243) gene has been shown to encode *Mt*MCAT. Interestingly, $FabD_2$ (Rv0649) is a novel gene, which also encodes a putative MCAT, although the $FabD_2$ gene product shares low sequence similarity with other MCATs.[14,15] $FabD_2$ also differs from FabD in secondary structure in different pH buffers, but is consistent with the function of reported MCATs in biosynthesis and possesses the typical activity of bacterial MCATs.[15] A significant strategy for the development of anti-bacterial drugs may be to search for lead compounds that simultaneously inhibit the two MCATs from *M. tuberculosis*.

Traditional remedies are unable to keep up with the threat posed by TB. To design and discover new anti-TB drugs is therefore essential, and the preferred strategy is to destroy the synthesis of fatty acids. For example, thiolactomycin (TLM) targets two b-ketoacyl-acyl-carrier protein synthases, KasA and KasB, which belong to the type II fatty acid synthases.[5,16] Because TLM inhibits the FAS II enzyme in different bacterial species, it has good potential to be developed into a broad-spectrum antibiotic that can be used to treat various bacterial infections including TB.[17] MCAT, as a key upstream enzyme in the fatty acid synthesis pathway, is another main target for the design of new therapeutics against TB. Pharmacological development based on three-dimensional structure can greatly enhance the success rate and efficiency of drug design. To date, the crystal structures of MCAT from *Escherichia coli* (*Ec*MCAT; PDB code: 1MLA)[18] and *Streptomyces coelicolor* (*Sc*MCAT; PDB code: 1NM2)[11] have been determined. Here we report the crystal structure of *Mt*MCAT to 2.3 Å resolution, in order to further elucidate the mechanism of fatty acid biosynthesis and provide an important structural basis for the discovery of new anti-TB drugs.

Results and Discussion

Overall structure of *Mt*MCAT

*Mt*MCAT crystals belong to the space group $P2_1$ with one molecule in the asymmetric unit. The crystal structure of *Mt*MCAT was solved using molecular replacement and refined to 2.3 Å resolution with R_{work} and R_{free} values of 19.8% and 23.8%, respectively (Table 1). The final model contains residues 1 to 301 of the full-length *Mt*MCAT protein and only Leu302 is not defined in the electron density map. One histidine residue was located before the first methionine in our structure and arose from the use of NdeI as the N-terminal restriction enzyme to clone FabD cDNA into the pET-28a vector. The final refined structure also includes 330 water molecules and one acetate molecule (ACY).

This 30 kDa *Mt*MCAT monomer is composed of two subdomains. The larger subdomain has a hydrolase core and comprises of residues 1–127 and 196–301, with 12 α-helices surrounding a core of four parallel β-strands. The smaller ferredoxin-like subdomain contains residues 128–195 and is made up of four antiparallel β-strands and two helices (Figure 1). The subdomains are linked to each other by two loops, serving as a hinge to clasp the acetate and the active site (Figure 1).

Sequence alignment shows that *Mt*MCAT shares 52% identity and 64% positive identity with *Sc*MCAT in primary sequence. The three-dimensional structures of these two proteins are closely related, although some notable differences are observed.

Table 1. X-ray data collection and refinement statistics

Parameters	Wild-type *Mt*MCAT
Data collection	
Cell parameters	a=37.0, b=48.9, c=77.9, α=γ=90.0°, β=98.7°
Space group	$P2_1$
Resolution (Å)[a]	50.0–2.3 (2.38–2.3)
No. of reflections	98,005
No. of unique reflections	14,232
Completeness (%)[a]	99.8 (99.1)
Average $I/\sigma(I)$[a]	11.1 (5.6)
R_{merge}[a,b]	8.1 (45.5)
Refinement	
No. of reflections (> 0 σ(*F*))	12,117
R_{work}[c]	19.76
R_{free} (5% data)	23.79
r.m.s.d. bond distance (Å)	0.005
r.m.s.d. bond angle (°)	1.16
Average *B*-value/all non-hydrogen atoms (Å^2)	37.3
Solvent atoms	330
Ramachandran plot (excluding proline and glycine)	
Residues in most favored regions	165 (92.0%)
Additional allowed regions	15 (7.6%)
Generously allowed regions	1 (Ser91, 0.4%)

[a] Values in parentheses correspond to the highest resolution shell.
[b] $R_{merge}=\sum_h\sum_i | I_i(h) - \langle I(h)\rangle | / \sum_h\sum_I I_i(h)$, where $\langle I(h)\rangle$ is the mean of the observations $I_i(h)$ of reflection h.
[c] $R_{work}=\sum (||F_{obs}|-F_{calc}||)/ \sum|F_{obs}|$; R_{free} is the R factor for a subset (10%) of reflections that was selected prior to refinement calculations and not included in the refinement.

The most significant difference is the loss of electron density in the *Sc*MCAT structure from residues 77 to 86, which may account for a very flexible loop. In our *Mt*MCAT structure, however, there is no absence of electron density in this region, which is most likely due to the formation of a shorter and more stable loop by residues 76 to 78. Other differences are evident on the surface of the protein, which do not seem to have an effect on enzyme activity. *Mt*MCAT also shares 32% identity and 56% positive identity with *Ec*MCAT in primary sequence and their structures also have very similar folds, with some notable differences at the surface.

One acetate bound to *Mt*MCAT

The structural data for the native enzyme were collected from a crystal grown in sodium acetate and clearly indicate that a single acetate molecule is bound to *Mt*MCAT (Figure 2). In contrast, two acetate molecules from the crystallization buffer are found in the *Sc*MCAT structure. The first acetate, termed ACY1, is bound to Gln9 and Arg122 in order to mimic the carboxyl end of a bound malonyl group. The second acetate, termed ACY2, stacks against the imidazole ring of His96 and is hydrogen bonded with the backbone carbonyl of Gln9.[11] In *Mt*MCAT, only one acetate equivalent to ACY1 is found in the active site where it interacts with the NH1 atom of Arg116 at a distance of 2.79 Å. This acetate molecule, hereafter named ACY, is also stabilized through a hydrogen bond between the O atom and the His194 $N^{\varepsilon 2}$ atom (3.10 Å) and through a weak interaction with the Gln9 $N^{\varepsilon 2}$ atom (3.15 Å), whereas a stronger interaction occurs between ACY1 and residue Gln9 of *Sc*MCAT (2.51 Å). Significantly, the ACY1 molecule of *Sc*MCAT binds very close to the active Ser97 (2.40 Å), while in *Mt*MCAT the ACY molecule is located more than 4.10 Å from the active Ser91. This observation concerning the placement of ACY is consistent with the previous report by Oefner and colleagues,[19] in which the catalytic serine residue is shown not to be involved in intermolecular hydrogen bond formation, either in the complex with glycerol or in the complex with malonate. Our reservoir buffer also contains acetate; however, when crystals were grown in the crystallization buffer in the absence of acetate, a single acetate was still observed bound in the same site of *Mt*MCAT. Interestingly, after soaking crystals with substrates or inhibitors, the resulting *Mt*MCAT structures showed no small molecules bound in the active site, although we cannot explain this phenomenon (data not shown). In each case, Ser91 and other active site residues possess the same conformation as the structure described here, indicating that ACY does not influence the spatial arrangement of the surrounding residues. The precise interaction between enzyme and substrate should be elucidated by further experiments, although the ACY molecule can be considered as a substrate mimic due to its similarity to malonate.[11]

The active pocket of *Mt*MCAT

The active site of *Mt*MCAT is located in a cavity between the large and small domains. The catalytic Ser91 residue belongs to a highly conserved GXSXG motif, which forms a tight turn between α6 and β2, known as the nucleophilic elbow. In *Sc*MCAT,

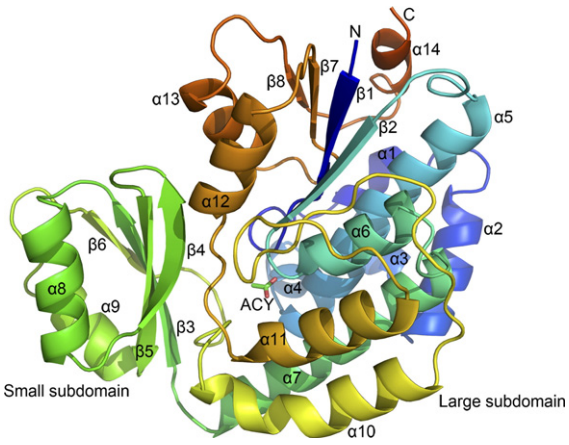

Figure 1. Overall structure of *M. tuberculosis* MCAT (*Mt*MCAT). The ferredoxin-like small subdomain is shown on the left and the large hydrolase subdomain is on the right. The structure is shown in ribbon representation and colored from blue at the N terminus to red at the C terminus. Secondary structure elements are labeled. One acetate molecule (ACY) is bound into the active pocket.

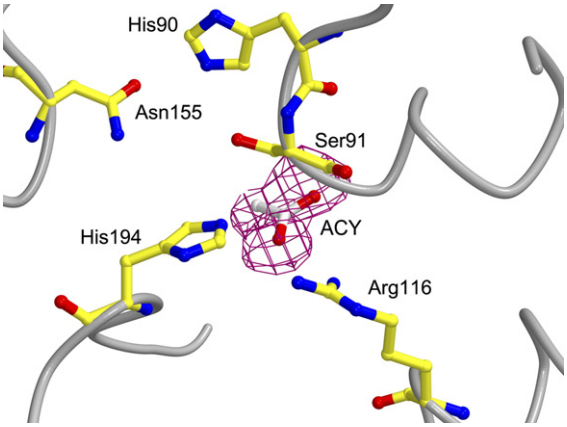

Figure 2. ACY binding to the active site of *Mt*MCAT. Active-site region together with the ACY at the final 2 $|F_o|-|F_c|$ electron density map (shown in pink mesh) contoured at 1.0 σ. The ACY is colored by white C and red O.

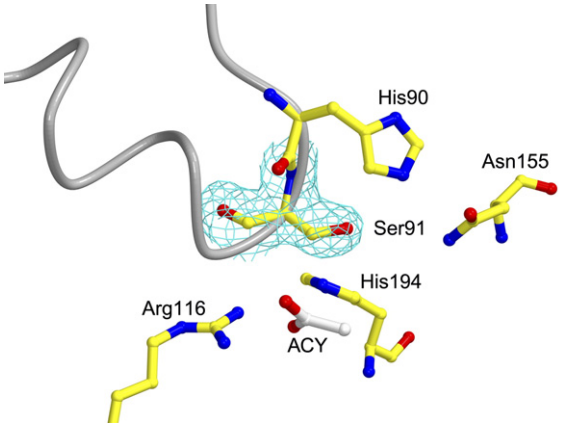

Figure 4. Electron density map covering the catalytic Ser91. The final 2 $|F_o|-|F_c|$ electron density map (shown in green mesh) contoured at 1.5 σ. Ser91 fits the electron density map very well.

the active Ser97 residue is stabilized by a 2.91 Å hydrogen bond between the NH2 atom of Arg122 and the O^{γ} atom of Ser97,[11] whereas the active Ser92 residue in *Ec*MCAT is stabilized by a water molecule.[18] In both the *Sc*MCAT and *Ec*MCAT structures, the active C^{β}–O^{γ} bond of serine is almost perpendicular to the imidazole ring of His201. In contrast, the C^{β}–O^{γ} bond of Ser91 in *Mt*MCAT is oriented upwards by ~100° to become almost parallel to the imidazole ring of His194 (Figure 3). The orientation of the Ser91 C^{β}–O^{γ} bond also results in significant changes in the active pocket of *Mt*MCAT compared with other MCAT structures. From a careful analysis of the crystal structure of *Mt*MCAT, it is evident that Ser91 and other residues in the active pocket fit the electron density map very well (Figure 4) and the mean temperature factor of Ser91 is low (~ 20.8 $Å^2$), suggesting that the orientation of Ser91 in our structure is correct and credible.

His90-Ser91 catalytic dyad

The change in orientation of the active Ser91 C^{β}–O^{γ} bond in *Mt*MCAT results in a change in the

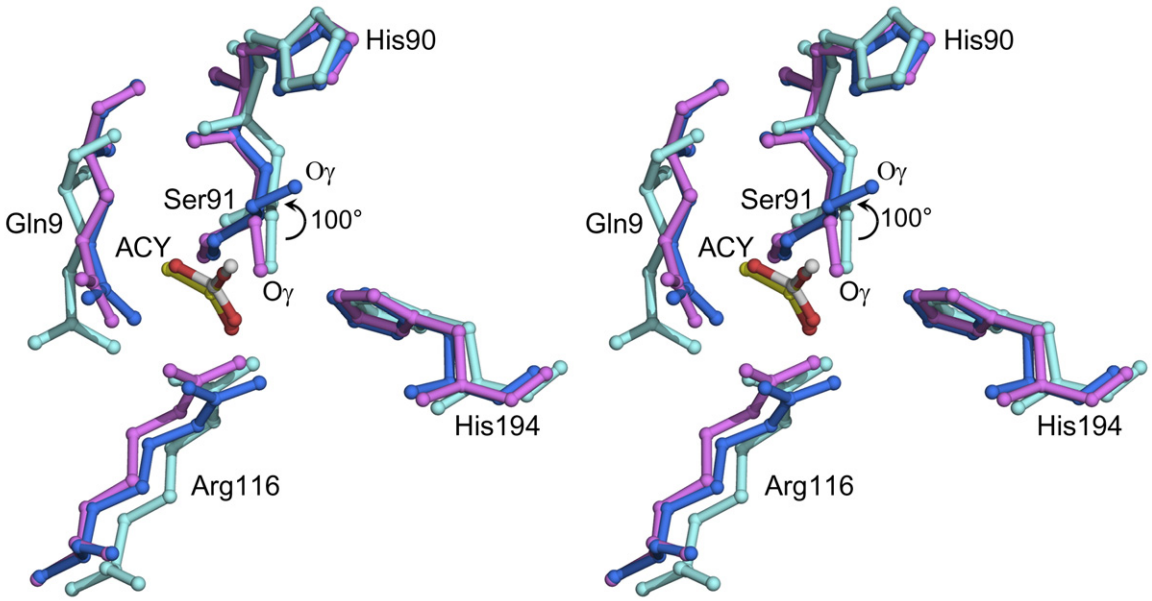

Figure 3. Stereo superposition of the active site of *Mt*MCAT, *Ec*MCAT and *Sc*MCAT. *Mt*MCAT is represented by marine sticks, *Ec*MCAT is represented by aquamarine sticks, and *Sc*MCAT is represented by violet sticks. The ACY molecule from the *Mt*MCAT structure is shown in yellow and the ACY1 molecule from the *Sc*MCAT structure is shown in grey. The C^{β}–O^{γ} bond of Ser91 from *Mt*MCAT is rotated upwards by about 100° (indicated by arrows).

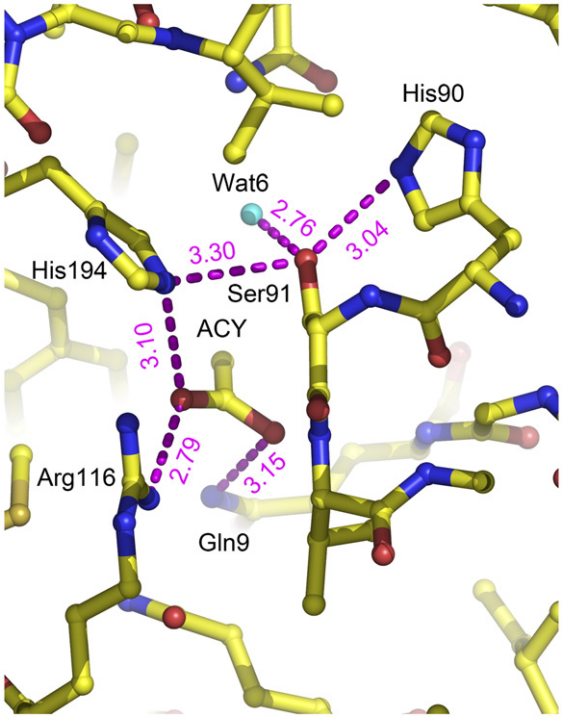

Figure 5. The relationship between residues and small molecules in the active site. The distance between His90 and Ser91 is 3.04 Å, which is shorter than the distance (3.30 Å) between His194 and Ser91, implying that His90 and not His 194 forms a dyad with Ser91, the active residue in *Mt*MCAT. Ser91 is stabilized by one water molecule (Wat6). The ACY molecule, which mimics the malonyl group of the substrate, is stabilized by Arg116, Gln9 and His94. The purple broken lines represent hydrogen bonds.

whole spatial relationship of the active pocket compared with *Sc*MCAT and *Ec*MCAT. In our *Mt*MCAT structure, the distance between the $N^{\varepsilon 2}$ atom of His90 and the O^{γ} atom of Ser91 is about 3.04 Å. In contrast, the respective distances in the *Sc*MCAT and *Ec*MCAT structures are greater than 5 Å. The distance between Ser91 and His194 in *Mt*MCAT is 3.3 Å, but the corresponding distance is only 2.66 Å and 2.83 Å in *Sc*MCAT and *Ec*MCAT, respectively. As a result, the active Ser91 residue in *Mt*MCAT is more conversant with His90 than with His194 (Figure 5). According to a previous report, Ser97 is the primary nucleophile in the active site of *Sc*MCAT, whereas His96 is a surrogate nucleophile and His201 plays the role of a general base in the serine-histidine catalytic dyad of the enzyme.[20] In the *Mt*MCAT structure, however, His90 (corresponding to His91 and His96 in *Ec*MCAT and *Sc*MCAT, respectively) is not a surrogate nucleophile but a key component for nucleophilic attack. The active site Ser91 is the exclusive catalytic residue, and it is His90 rather than His194 that forms a catalytic dyad with Ser91. The distance between the $N^{\varepsilon 2}$ atom of His194 and the O^{γ} atom of Ser91 (3.3 Å) is too far to form any bond and serine will preferentially select the closest histidine as its partner to initiate nucleophilic attack. So, in the *Mt*MCAT structure, Ser91 and His194 cannot form a catalytic dyad. Instead, His90 replaces His194 and the proton transfer chain is changed.

Asn155-Wat6-Ser91 nucleophilic attack chain

Interestingly, a second proton transfer chain found in the *Mt*MCAT structure is composed of Asn155, the water molecule Wat6 and Ser91 (Figure 6). The distance between Asn155 and Wat6 is 3.02 Å, while the distance between Wat6 and Ser91 is 2.76 Å (Figure 6). The water plays an important role in bridging Ser91 and Asn155, and thus can support proton transfer by accepting a proton from Ser91 and donating a proton to Asn155. As a consequence, the Ser91 residue can be polarized by Asn155 and initiate nucleophilic attack. A similar chain has also been observed in other structures. For instance, Kim and colleagues reported that in the precursor CAD structure, a water molecule (Wat1) donates a proton to a hydrogen acceptor (Asn244β) and accepts a proton from the hydroxyl group of Ser1β, thereby assisting in nucleophilic attack by the hydroxyl group of the serine in intramolecular cleavage.[21]

Asn155-His90-Ser91 nucleophilic attack chain

His90 is located 3.13 Å from Asn155 and could become negatively charged *via* the transfer of one proton to Asn155, thus initiating nucleophilic attack on the substrate. However, taking into consideration the placement of malonyl-CoA in the complex structure solved by Oefner and colleagues,[19] the His90-Asn155 nucleophilic attack dyad cannot occur at this site because the distance between His90 and the substrate is too far for nucleophilic attack. We

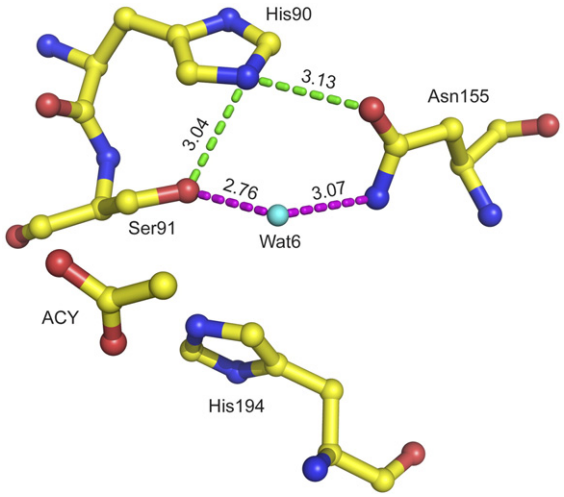

Figure 6. Asn155-Wat6-Ser91 and Asn155-His90-Ser91 nucleophilic attack chains. The green dash represents the Asn155-His90-Ser91 proton transfer chain and the purple dash represents the Asn155-Wat6-Ser91 proton transfer chain. The two chains are not found in the *E. coli* or *S. coelicolor* MCAT structures.

therefore propose a third nucleophilic attack chain comprised of Asn155-His90-Ser91 (Figure 6). We postulate that the lone residue (His90), as in several other serine hydrolases, is sufficient to activate Ser91 for direct nucleophilic attack on the substrate,[21–26] but additional interactions may assist His90 in activating Ser91. Wang and colleagues reported a water-mediated hydrogen bond between His254 and Asn251 to assist in polarizing the active Ser201 in the crystal structure of rhomboid family intramembrane protease.[27] In our structure, His90 and Asn155 are within direct hydrogen bonding distance and do not require the presence of a water molecule to mediate the interaction. His90, polarized by Asn155, could accept one proton from Ser91, which would then become negatively charged through the loss of a proton, enabling it to initiate a nucleophilic attack on the substrate.

Enzyme activity assays

After locating three potential new proton transfer chains in *Mt*MCAT, we constructed three mutants, H90A, N155A and H90A-N155A, for enzyme activity assays in order to clarify their roles in the active site of *Mt*MCAT. In a series of experiments, the concentration of holo-AcpM was kept constant while different concentrations of malonyl-CoA were introduced into the reaction mixture. All data were input into the software OriginPro7.5 (OriginLab Corporation) for automatic calculation of the Hill parameters (Table 2) and plotting of curves (Figure 7). Since the activity of the double mutant H90A-N155A is too low to be measured accurately, the data are not shown here. The results of our enzyme activity assays show little difference between the K_m of wild-type and mutant MCATs, although there are substantial differences in their V_{max}. Of the three mutants assayed, the double mutant has the lowest activity, followed by H90A. The catalytic activity of N155A is the highest of the three mutants assayed and is approximately 50% of the activity of the wild-type enzyme. These results provide strong evidence to support our hypothesis that His90 serves as the base in the Ser-His catalytic dyad, while Asn155 enhances the proton transfer ability of His90. Mutating His90 to alanine causes MCAT to undergo a substantial loss of activity, but the mutant still retains weak activity because the Asn155-Wat6-Ser91 chain is unperturbed and can support the catalytic process. When Asn155 is mutated to alanine, the activity is reduced to half of the wild type MCAT activity, but it retains higher activity than the H90A mutant. This suggests that Asn155 can participate in nucleophilic attack, but is not a critical residue and its function is accessorial. The double mutant undergoes a complete loss of activity, since all three proton transfer chains are abolished. Ser91 could not be polarized without His90 and Asn155, which is consistent with our structural observations. The wild-type and mutant MCATs all possess similar K_m values, indicating that His90 and Asn155 are not responsible for substrate binding or recognition.

Table 2. Comparison of K_m and V_m for wild-type *Mt*MCAT and mutants with malonyl-CoA as substrate

Type	Wild-type	His90A	Asn155A	His90A-Asn155A
K_m (μM)	16.77	19.11	17.55	—
V_m (RFU/min)	123.01	39.65	63.06	—

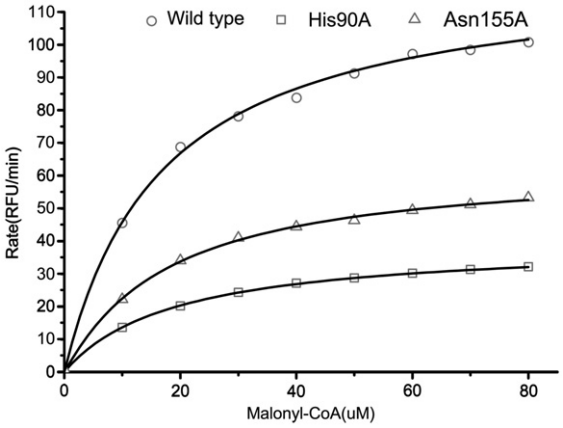

Figure 7. Kinetic analysis of wild-type *Mt*MCAT and mutants towards malonyl-CoA using a fluorometric coupled enzyme assay. Data for wild-type *Mt*MCAT and H90A and N155A mutants are shown. No data is shown for the H90A-N155A double mutant as the activity was too low to measure accurately.

We observe three new protein transfer pathways from our *Mt*MCAT structure, none of which is identical to the classical pathway identified from structures of *Ec*MCAT and *Sc*MCAT. In the *Sc*MCAT structure, there is no water molecule linking Asn161 and Ser97 for proton transfer and the two residues are located far away from each other. In *Ec*MCAT, although there is one water molecule between the equivalent asparagine and serine residues, they are also too far to support proton transfer. Analysis of the Ramachandran plot (Table 1) shows that Ser91 is located in a generously allowed region, suggesting that the orientation of Ser91 might be influenced by strong interactions. Both Wat6 and His90 interact with the serine, effectively pulling the C^{β}–O^{γ} bond of Ser91 and turning it towards them. With no interactions on the other side of the C^{β}–O^{γ} bond of Ser91 to balance these interactions, except for one weak interaction between His194 and Ser91, the net result is that the C^{β}–O^{γ} bond of Ser91 is rotated by ~100° relative to the equivalent serine in other similar MCAT structures (Figure 3). This reorientation of the Ser91 C^{β}–O^{γ} bond destroys the classical His194-Ser91 catalytic dyad and establishes three new proton transfer chains for catalysis: His90-Ser91, Asn155-Wat6-Ser91 and Asn155-His90-Ser91.

As a result, the catalytic mechanisms of *Mt*MCAT differ from the classical mechanism of *Sc*MCAT and *Ec*MCAT. *Mt*MCAT catalyzes malonate transfer *via* a ping-pong bi-bi mechanism using serine as a catalytic residue. When malonyl-CoA binds to the enzyme, the Arg116 and His194 residues recognize and stabilize it. The thioester carbonyl of the malonyl carboxylate group inserts into the oxyanion hole created by glutamine and valine. At the same time, Ser91 is polarized by His90 or Asn155 through Wat6, and initiates a nucleophilic attack on the thioester carbonyl in order to liberate CoA from malonyl-MCAT. Subsequently, holo-ACP binds to the enzyme and the malonate is transferred to holo-ACP from the malonyl-MCAT intermediate.

Our biochemical experiments and those of our colleagues provide further evidence for the three proton transfer chains proposed here. A study by Kremer *et al.* reports that the H194A mutant of *Mt*MCAT is unable to bind malonyl-CoA but does possess catalytic activity, albeit considerably lower than the wild-type *Mt*MCAT. Indeed, the catalytic activity of the H194A mutant is higher than for other mutants, including Q9A, R116A, Q243A, S91T and S91A. Of these, only S91A completely loses its catalytic activity. All of these observations suggest that residue His194 of *Mt*MCAT is not a component of the catalytic dyad or triad and does not participate in nucleophilic attack. Instead, our structural analysis indicates that its role should be to bind and stabilize the substrate. The decreased catalytic activity of the H194A mutant can therefore be explained by its decreased substrate binding ability.[28] As His194 cannot assist Ser91 to initiate nucleophilic attack, other proton transfer chains are required to replace the His194-Ser91 dyad in order to achieve nucleophilic attack. His90-Ser91 is the most likely choice, and our enzyme kinetic assays of wild-type *Mt*MCAT and mutants indicate that H90A undergoes a greater loss of activity than N155A, but does not completely lose activity. These observations are consistent with the existence of three new proton transfer chains. His90 acts as the base for nucleophilic attack with Ser91, while Asn155 can also accept a proton from Ser91 *via* His90 or Wat6. The existence of three new chains in *Mt*MCAT is not concurrent and, without further experimental evidence, it is not clear which is the predominant proton transfer chain. Based on our enzyme kinetic assay results, we postulate that His90-Ser91 should be the most important chain.

Conclusions

Our structural studies of *Mt*MCAT indicate a strikingly different catalytic mechanism from other known MCAT enzymes. *M. tuberculosis* can survive and replicate in the hostile environment of host macrophages because of its thick cell membranes, which protects it from lethal microbicidal molecules. Our structural analysis of *Mt*MCAT could provide useful insights into the mechanistic basis for this unusual flexibility in the choice of nucleophilic attack chains in the active site of the enzyme. The three possible catalytic pathways shown here differ from all other reported pathways for MCAT enzymes. This difference may be important for the production of thicker and stronger membranes by *M. tuberculosis*, and may aid the design of inhibitors specific to *Mt*MCAT.

Materials and Methods

Expression and purification of *M. tuberculosis* MCAT

A cDNA fragment (FabD) encoding *M. tuberculosis* MCAT was cloned into the bacterial expression vector pET28a (Novagen) with a His tag at the N terminus. The recombinant plasmid was transformed into *E. coli* strain BL21 (DE3) and over-expressed. Cells were cultured at 310 K in 1 l of LB medium containing 50 mg ml^{-1} kanamycin to an A_{600nm} of 0.6–0.8. The cells were then induced with 1 mM isopropyl-β-D-thiogalactopyranoside (IPTG) and continuously incubated at 310 K for a further 4 h to an A_{600nm} of 2.0. The cells were harvested by centrifugation, resuspended in lysis buffer (20 mM Tris–HCl (pH 7.9), 500 mM NaCl, 5 mM imidazole, 10% (v/v) glycerol) and homogenized by sonication. The soluble cell lysate obtained by centrifugation at 15,000*g* for 30 min was applied onto a Ni^{2+}-chelating affinity column (1.5 ml Ni^{2+}–NTA agarose) pre-equilibrated with lysis buffer. The contaminant protein was thoroughly washed off with wash buffer (20 mM Tris–HCl (pH 7.9), 500 mM NaCl, 20 mM imidazole, 10% glycerol) for at least ten bed volumes and the target protein was eluted with 20 mM Tris–HCl (pH 7.9), 500 mM NaCl, 200 mM imidazole, 10% glycerol for about 10 ml. The eluted sample was then concentrated using an Ultrafree 10,000 NMWL filter unit (Millipore) to 500 μl and further applied onto a Superdex-75 size-exclusion chromatography column (Pharmacia) with buffer A (20 mM Tris–HCl (pH 7.5), 150 mM NaCl). The target peak corresponding to a molecular weight of about 30 kDa (a monomer) was collected and loaded onto a Resource Q anion-exchange chromatography column (Pharmacia) equilibrated with buffer B (20 mM Tris–HCl (pH 7.5), 100 mM NaCl). After washing the unbound protein with three bed volumes, a linear gradient of 0.1–1.0 M NaCl in the same buffer was applied. MCAT was finally eluted with approximately 0.35 M NaCl. The purified sample was concentrated and transferred into a buffer containing 20 mM Tris–HCl (pH 7.5) and 50 mM NaCl. The purity of protein was then analyzed on SDS–PAGE (better than 90% purity) and was judged to be suitable for crystallization.

Construction of MCAT mutants

The MCAT His90A mutant was constructed by replacing the CAC codon for His90 with GCC. The mutant Asn155A was constructed by replacing the AAC codon for Asn155 with GCC. The MCAT His90A-Asn155A double mutant was constructed by simultaneously replacing the CAC and AAC codons with GCC. All constructs were transformed into *E. coli* strain BL21 (DE3). The expression and purification protocols are the same as for the wild-type enzyme described above.

Crystallization and X-ray data collection

The purified protein was concentrated using an Ultrafree 10,000 NMWL filter unit (Millipore) to 25 mg ml^{-1} in a solution containing 20 mM Tris–HCl (pH 7.5), 30 mM NaCl. The preliminary crystallization conditions were obtained by the sparse-matrix sampling technique[29] with the hanging-drop vapour-diffusion method using Crystal Screen I and Crystal Screen II reagent kits (Hampton Research). Crystals suitable for X-ray diffraction were obtained from 30% (w/v) PEG 4000, 0.1 M Tris–HCl (pH 8.5), 0.2 M sodium acetate. 1 μl of protein solution was mixed with 1 μl of reservoir solution and equilibrated against 200 μl of reservoir solution at 291 K. Crystals grew in two weeks and initially diffracted to 4.0 Å resolution, but following optimization they grew in four to five days and diffracted to at least 2.5 Å resolution.

X-ray diffraction data for the *M. tuberculosis* MCAT protein were collected in-house at 291 K using a Rigaku MM-007 X-ray generator ($\lambda = 1.5418$ Å) and a Mar345dtb detector. The crystal was flash cooled for data collection and no cryoprotectant was used. Diffraction data were integrated, scaled and merged using the program HKL2000.[30]

Structure determination and refinement

Initial phases were obtained by molecular replacement with the program CNS.[31] The search model consisted of a single MCAT monomer from the previous *Sc*MCAT structure (PDB code: 1NM2). Model building was performed iteratively in O[32] with rounds of simulated annealing, energy minimization, and *B* factor refinement in CNS. The figures were drawn using PYMOL (DeLano Scientific, San Carlos, CA). Data collection and refinement statistics are summarized in Table 1.

Coupled enzyme assay

The purified wild-type and mutant enzymes were subjected to enzyme characterization using the coupled enzyme method[33] with minor modifications. All enzymatic reactions were conducted in a final volume of 100 μl and performed in 96-well microtiter plates using Fluoroskan Ascent (Thermo Electron Corporation). Enzymes were diluted to twice the final assay concentration in 50 mM phosphate buffer (pH 6.8), 1 mM EDTA, 1 mM DTT, and 0.1 mg/ml BSA. Malonyl-CoA was prepared at four times the final assay concentration in 50 mM phosphate buffer (pH 6.8), 1 mM EDTA, 1 mM DTT. ACP and PDH (pyruvate dehydrogenase) were diluted together at four times their final concentrations in the same buffer supplemented with 8 mM pyruvic acid, 1 mM NAD, and 0.8 mM TPP. The final concentrations of all ingredients were 50 mM phosphate buffer (pH 6.8), 1 mM EDTA, 1 mM DTT, 2 mM pyruvic acid, 0.25 mM NAD, 0.2 mM TPP, 0.03 nM MCAT, 60 μM ACP, 15 munits/100 μl PDH, and 25 μM malonyl–CoA. All solutions and the microplate reader were pre-equilibrated at 37 °C. The components were pipetted in the following order: 50 μl MCAT solution, 25 μl ACP/PDH mix, and then 25 μl malonyl–CoA solution to start the reaction. NADH fluorescence was immediately measured at the excitation wavelength (340 nm) and the emission wavelength (465 nm) for 5 min.

Protein Data Bank accession code

The ataomic coordinates have been deposited in the RCSB and are available under accession code 2QC3.

Acknowledgements

This project was supported by the following grants: State "863" High-Tech Project (Grant No. 2005BA711A05-02), "973" Project (Grant Nos. 2006CB806503 and 2002CB512804), the NSFC (Grant No. 30221003), the Ministry of Education (Grant No. V200611), and the Knowledge Innovation Project of the Chinese Academy of Sciences (Grant No. KSCX1-YW-R-05).

References

1. Brennan, P. J. & Nikaido, H. (1995). The envelope of mycobacteria. *Annu. Rev. Biochem.* **64**, 29–63.
2. Minnikin, D. E. (1982). Lipids: complex lipids, their chemistry, biosynthesis and roles. In *The Biology of the Mycobacteria* (Ratledge, C. & Stanford, J., eds), pp. 95–184, Academic Press, New York.
3. Banerjee, A., Dubnau, E., Quemard, A., Balasubramanian, V., Um, K. S., Wilson, T. *et al.* (1994). inhA, a gene encoding a target for isoniazid and ethionamide in *Mycobacterium tuberculosis*. *Science*, **263**, 227–230.
4. Dessen, A., Quemard, A., Blanchard, J. S., Jacobs, W. R., Jr & Sacchettini, J. C. (1995). Crystal structure and function of the isoniazid target of *Mycobacterium tuberculosis*. *Science*, **267**, 1638–1641.
5. Kremer, L., Douglas, J. D., Baulard, A. R., Morehouse, C., Guy, M. R., Alland, D. *et al.* (2000). Thiolactomycin and related analogues as novel anti-mycobacterial agents targeting KasA and KasB condensing enzymes in *Mycobacterium tuberculosis*. *J. Biol. Chem.* **275**, 16857–16864.
6. Quemard, A., Sacchettini, J. C., Dessen, A., Vilcheze, C., Bittman, R., Jacobs, W. R., Jr & Blanchard, J. S. (1995). Enzymatic characterization of the target for isoniazid in *Mycobacterium tuberculosis*. *Biochemistry*, **34**, 8235–8241.
7. Slayden, R. A., Lee, R. E. & Barry, C. E., 3rd (2000). Isoniazid affects multiple components of the type II fatty acid synthase system of *Mycobacterium tuberculosis*. *Mol. Microbiol.* **38**, 514–525.
8. Campbell, J. W. & Cronan, J. E., Jr (2001). Bacterial fatty acid biosynthesis: targets for antibacterial drug discovery. *Annu. Rev. Microbiol.* **55**, 305–332.
9. White, S. W., Zheng, J., Zhang, Y. M. & Rock (2005). The structural biology of type II fatty acid biosynthesis. *Annu. Rev. Biochem.* **74**, 791–831.
10. Arthur, C. J., Szafranska, A., Evans, S. E., Findlow, S. C., Burston, S. G., Owen, P. *et al.* (2005). Self-malonylation is an intrinsic property of a chemically synthesized type II polyketide synthase acyl carrier protein. *Biochemistry*, **44**, 15414–15421.
11. Keatinge-Clay, A. T., Shelat, A. A., Savage, D. F., Tsai, S. C., Miercke, L. J., O'Connell, J. D., 3rd *et al.* (2003). Catalysis, specificity, and ACP docking site of *Streptomyces coelicolor* malonyl-CoA:ACP transacylase. *Structure*, **11**, 147–154.

12. Summers, R. G., Ali, A., Shen, B., Wessel, W. A. & Hutchinson, C. R. (1995). Malonyl-coenzyme A:acyl carrier protein acyltransferase of *Streptomyces glaucescens*: a possible link between fatty acid and polyketide biosynthesis. *Biochemistry*, **34**, 9389–9402.
13. Liu, W., Han, C., Hu, L., Chen, K., Shen, X. & Jiang, H. (2006). Characterization and inhibitor discovery of one novel malonyl-CoA: acyl carrier protein transacylase (MCAT) from *Helicobacter pylori*. *FEBS Letters*, **580**, 697–702.
14. Cole, S. T., Brosch, R., Parkhill, J., Garnier, T., Churcher, C., Harris, D. *et al.* (1998). Deciphering the biology of *Mycobacterium tuberculosis* from the complete genome sequence. *Nature*, **393**, 537–544.
15. Huang, Y. S., Ge, J., Zhang, H. M., Lei, J. Q., Zhang, X. L. & Wang, H. H. (2006). Purification and characterization of the *Mycobacterium tuberculosis* FabD2, a novel malonyl-CoA:AcpM transacylase of fatty acid synthase. *Protein Expr. Purif.* **45**, 393–399.
16. Slayden, R. A., Lee, R. E., Armour, J. W., Cooper, A. M., Orme, I. M., Brennan, P. J. & Besra, G. S. (1996). Antimycobacterial action of thiolactomycin: an inhibitor of fatty acid and mycolic acid synthesis. *Antimicrob. Agents Chemother.* **40**, 2813–2819.
17. Zhang, Y. & Amzel, L. M. (2002). Tuberculosis drug targets. *Curr. Drug Targets*, **3**, 131–154.
18. Serre, L., Verbree, E. C., Dauter, Z., Stuitje, A. R. & Derewenda, Z. S. (1995). The *Escherichia coli* malonyl-CoA:acyl carrier protein transacylase at 1.5-Å resolution. Crystal structure of a fatty acid synthase component. *J. Biol. Chem.* **270**, 12961–12964.
19. Oefner, C., Schulz, H., D'Arcy, A. & Dale, G. E. (2006). Mapping the active site of *Escherichia coli* malonyl-CoA-acyl carrier protein transacylase (FabD) by protein crystallography. *Acta Crystallog. sect. D*, **62**, 613–618.
20. Dreier, J., Li, Q. & Khosla, C. (2001). Malonyl-CoA: ACP transacylase from *Streptomyces coelicolor* has two alternative catalytically active nucleophiles. *Biochemistry*, **40**, 12407–12411.
21. Kim, Y., Kim, S., Earnest, T. N. & Hol, W. G. (2002). Precursor structure of cephalosporin acylase. Insights into autoproteolytic activation in a new N-terminal hydrolase family. *J. Biol. Chem.* **277**, 2823–2829.
22. Paetzel, M., Dalbey, R. E. & Strynadka, N. C. (1998). Crystal structure of a bacterial signal peptidase in complex with a beta-lactam inhibitor. *Nature*, **396**, 186–190.
23. Tjalsma, H., Stover, A. G., Driks, A., Venema, G., Bron, S. & van Dijl, J. M. (2000). Conserved serine and histidine residues are critical for activity of the ER-type signal peptidase SipW of *Bacillus subtilis*. *J. Biol. Chem.* **275**, 25102–25108.
24. Wei, Y., Schottel, J. L., Derewenda, U., Swenson, L., Patkar, S. & Derewenda, Z. S. (1995). A novel variant of the catalytic triad in the *Streptomyces scabies* esterase. *Nature Struct. Biol.* **2**, 218–223.
25. Zhou, G. W., Guo, J., Huang, W., Fletterick, R. J. & Scanlan, T. S. (1994). Crystal structure of a catalytic antibody with a serine protease active site. *Science*, **265**, 1059–1064.
26. Fersht, A. (1999). *Structure and Mechanism in Protein Science: a Guide to Enzyme Catalysis and Protein Folding.* Freeman, W. H., New York.
27. Wang, Y., Zhang, Y. & Ha, Y. (2006). Crystal structure of a rhomboid family intramembrane protease. *Nature*, **444**, 179–180.
28. Kremer, L., Nampoothiri, K. M., Lesjean, S., Dover, L. G., Graham, S., Betts, J. *et al.* (2001). Biochemical characterization of acyl carrier protein (AcpM) and malonyl-CoA:AcpM transacylase (mtFabD), two major components of *Mycobacterium tuberculosis* fatty acid synthase II. *J. Biol. Chem.* **276**, 27967–27974.
29. Jancarik, J. & Kim, S.-H. (1991). Sparse matrix sampling: a screening method for crystallization of proteins. *J. Appl. Crystallog.* **24**, 409–411.
30. Otwinowski, Z. & Minor, W. (1997). Processing of X-ray diffraction data collected in oscillation mode. In *Macromolecular Crystallography,* part A (Carter, C. W., Jr & Sweet, R. M., eds), vol. 276, pp. 307–326. Academic Press.
31. Brunger, A. T., Adams, P. D., Clore, G. M., DeLano, W. L., Gros, P., Grosse-Kunstleve, R. W. *et al.* (1998). Crystallography & NMR System: a new software suite for macromolecular structure determination. *Acta Crystallog. sect. D*, **54**, 905–921.
32. Jones, T. A., Zou, J. Y., Cowan, S. W. & Kjeldgaard, M. (1991). Improved methods for building protein models in electron density maps and the location of errors in these models. *Acta Crystallog. sect. A*, **47**, 110–119.
33. Molnos, J., Gardiner, R., Dale, G. E. & Lange, R. (2003). A continuous coupled enzyme assay for bacterial malonyl-CoA:acyl carrier protein transacylase (FabD). *Anal. Biochem.* **319**, 171–176.

Edited by M. Guss

(Received 6 March 2007; received in revised form 1 June 2007; accepted 4 June 2007)
Available online 9 June 2007